J Therm Spray Tech
https://doi.org/10.1007/s11666-026-02161-1

ORIGINAL RESEARCH ARTICLE

Residual Stress Depth Distributions in Cold Gas Sprayed Titanium Coatings—Effect of Nozzle Traverse Speed and Substrate Material

D. Gabani[1] · Z. Arabgol[2] · L. Wiehler[2] · A. List[2] · T. Klassen[2] · F. Gärtner[2] · A. Pundt[1] · J. Gibmeier[1]

Submitted: 14 February 2025 / in revised form: 20 October 2025 / Accepted: 18 November 2025

Abstract As a solid-state material deposition technique with unique capabilities concerning attainable properties, cold gas spraying (CGS) is gaining increasing attraction in application fields of functional coatings, additive manufacturing, and local component repair. In the present study, CGS of grade 1 titanium was investigated in view of application as a repair method of damaged aerospace components. The current study focuses mainly on analysing residual stresses developed in the deposited material and substrate by means of the incremental hole-drilling method. This work aimed to investigate the influence of local thermal contributions on residual stresses by focusing on nozzle traverse speed and the type of substrate material. The results indicate that local residual stresses depend on the thermal mismatch between coating and substrate materials, the substrate material properties, and the nozzle traverse speeds. For instance, the residual stresses in grade 1 titanium coatings were observed to be tensile in case of coating and substrate exhibiting similar thermal properties, and compressive (thermal stress dominant) in case of coating material having significantly lower coefficient of thermal expansion than the substrate. Additionally, it was observed that the residual stresses shifted further toward the tensile residual stress regime under increased surface temperature by using decreased nozzle traverse speeds.

✉ D. Gabani
dhruvit.gabani@kit.edu

[1] Institute for Applied Materials (IAM-WK), Karlsruhe Institute of Technology, Karlsruhe, Germany

[2] Institute of Materials Technology, Helmut Schmidt University, University of the Federal Armed Forces, Hamburg, Germany

Keywords cold gas spraying (CGS) · incremental hole-drilling · nozzle traverse speed · residual stresses · titanium coatings

Introduction

Fundamentally, cold gas spraying (CGS) is a material deposition technique, in which the material powder is injected into the stream of pressurized and heated gas (i.e., nitrogen or helium) and passes through a de Laval type (converging–diverging) nozzle, leading to the supersonic velocities of particles (Ref 1). In contrast to the conventional thermal spraying (i.e., plasma spraying, flame spraying, and arc spraying) in which the depositing material is molten, the deposition of material in cold gas spraying (CGS) is driven by high velocity impacts and takes place in solid state as the temperature of material particles is substantially below the melting temperature (Ref 1, 2). Therefore, CGS is highly suitable for heat and oxygen-sensitive materials as almost no phase transformation and oxidation occur. Bonding of high velocity solid particles in CGS is mainly attributed to localized adiabatic shear instabilities (due to higher degrees of deformation and associated heat rises) in the vicinity of particle–substrate or particle–particle interface and the mechanical interlocking of materials (Ref 3–8). The authors suggest that the bonding occurs at the particle–substrate or particle–particle interfaces.

In the aerospace sector, the strict regulations and specifications for desired properties cause the manufacturing of components an expensive and intricate process. However, while in service, the aerospace components are susceptible to various damages (e.g., fatigue, wear, corrosion, foreign object impact, and environmental degradation) and often

Published online: 02 April 2026

need to be replaced (Ref 9–11). Replacing a component is not an economically and environmentally favourable approach. Therefore, owing to the distinctive characteristics and unique advantages of CGS (i.e., lower thermal input during the process, almost no phase transformation, and little or no oxidation), it has emerged as a potential alternative for the repair or refurbishment of such damaged components as well as in coatings or surface enhancement (Ref 9). When the repair of the aerospace component is concerned, the mechanical integrity and properties of the repaired component must be retained. However, the residual stresses build up during the CGS process could influence overall repair quality (i.e., bonding strength, mechanical properties) and consequently the performance and lifetime of a repaired component. Hence, understanding the development of residual stresses induced is essential for a proper assessment of using the method for component repair.

Due to the favourable properties of titanium (Ti), such as good strength-to-density ratio, formability, and remarkable corrosion resistance; it is highly compatible for making complex parts and using as protective coatings, i.e., protecting the substrate material from corrosive attack and increasing its wear resistance (Ref 12). Given the challenges associated with spraying Ti using conventional thermal sprayings in which it is heated to a molten or semi-molten state, CGS has seemed to be a more effective method for spraying Ti (Ref 7). Furthermore, a good deposition efficiency and adhesion in cold gas spraying of Ti leads to the densely deposited coatings, and the strength of Ti also allows it to preserve residual stresses developed due to deposition without substantial stress relief, which makes it a well-suited model material for studying the effect of CGS process parameters on residual stress build-up.

The reports on stresses in CGS of different materials are rather diverse. In the early times, many compressive coating residual stresses in CGS were observed and mainly attributed to peening effects (Ref 13–19). More recent work reports more diverse results, with less pronounced compressive stress contributions, which might be attributed to equipment developments that enable higher gas and particle temperatures (Ref 10, 20–22). Some basic findings from these studies are briefly explained later in this section. In contrast to conventional thermal sprayings, compressive residual stresses have mostly been observed in CGS, attributed to the peening mechanism caused by particle impacts driven local plastic deformations during deposition (Ref 19, 23). This could enhance the suitability of CGS for repair applications, as in many cases, compressive residual stresses up to a certain extent are desirable and therefore often systematically incorporated near the surface of a component to improve its performance and lifetime during operation. In addition to the peening in CGS, the local temperature gradient at the particle impact zone might contribute to tensile thermal stresses build up in deposited material. Furthermore, thermal stresses are also introduced during post-deposition cooling of the coating system if the coating and substrate have different thermal contractions, i.e., different coefficients of thermal expansion (CTE). The final residual stress state in the cold gas sprayed component is therefore a superposition of deposition (or evolving) and thermal stresses, in which understanding the respective contributions and the influence of CGS process parameters on residual stress development is crucial to optimize them for repair and other CGS applications, e.g., the usage of Ti coatings as protective layers.

Boruah et al. performed residual stress analysis by means of neutron diffraction and the contour method in cold sprayed Ti-6Al-4V deposits (thickness: 1.5 mm and 4.5 mm) on Ti-6Al-4V substrates (thickness: 5 mm and 10 mm), deposited using N_2 as process gas at 1100 °C and 50 bar pressure (Ref 10). In their study, the authors found residual stresses to be highly tensile near the free surface of the coating and at the bottom of the substrate, while being compressive near the interface, which are only deposition stresses developed during spraying as there is no thermal mismatch (i.e., no post-deposition stress build-up) between deposited and substrate materials (Ref 10). However, Price et al. reported very low compressive residual stresses in commercially pure Ti coating deposited on grade 5 Ti-6Al-4V substrate while using He as process gas at room temperature and 30 bar pressure (Ref 24).

In (Ref 10, 21, 25, 26), it is reported how the nozzle traverse speed influences the heat transfer and consequently the residual stress state in cold gas sprayed coating-substrate systems. For example, Luzin et al. in (Ref 25) observed the deposition residual stresses being more tensile for lower nozzle speed in CGS deposited lean duplex stainless steel coatings of thickness ranging between 1.5 and 3.1 mm on 6.2 mm thick substrates of austenitic stainless steel 316. A similar trend was noted in (Ref 21), i.e., slowing down the robot (nozzle) traverse speed could shift the compressive residual stresses to tensile residual stresses in IN718 or IN625 coatings. The authors suggest that such trends might be attributed to the superposition of longer residence time of the nozzle (process gas) and increased amount of material deposition at the particle impact zone enhance local temperature gradient and leading to the higher tensile stresses.

Suhonen et al. in (Ref 22) attempted to distinguish between deposition and thermal stresses built up during cold gas spraying of Al, Cu, and Ti powder on carbon steel (S355), stainless steel (AISI316), and Al alloy (6061-T6) substrates using an in situ curvature measurement device

(ICP-sensor) equipped with three lasers for monitoring the curvature of the plate-like sample during deposition. In their study, it was observed that the deposition residual stresses in Ti coatings were all tensile, as the peening effect might be less pronounced. The influence of peening and thermal effect in CGS depends on the material system and process parameters such as gas temperature, gas pressure, etc. However, due to the large CTE difference between Ti coatings and the substrate mentioned above, compressive thermal stresses appeared to be dominating the final residual stress state. In their study, the residual stress depth profile in coatings was not discussed as one stress value representing the residual stress state in the coatings were given. Luzin et al. in (Ref 18, 27) determined through-thickness residual stress distribution using neutron diffraction stress analysis in Ti coatings deposited on Cu and Fe substrates using different CGS devices with different process gases, i.e., N2 (at 39 bar pressure and 615 °C temperature) and He (at 6.2 bar pressure and 365 °C temperature). Their study showed that the residual stresses in the Ti coatings were mostly compressive in the coating and dominated by thermal stresses due to the significant difference in the CTE of Ti, Fe, and Cu. Moreover, the compressive stresses were higher for higher gas temperatures.

The review of the state of the art shows that substantial work has been done in the field of residual stress development in cold gas spraying with variation of process parameters and coating system characteristics. However, systematic studies are still missing in particular with regard to finely resolved residual stress depth distributions and the contributions to the residual stress build-up, namely distinguishing peening and thermal effects. A combination of these contributions results in complex interaction and limits possible predictions of residual stress states. A systematic parameter study, while specifically addressing individual contributions can shed more light onto this complex interaction and will contribute to an enhanced comprehension of residual stress build-up.

In this regard, the grade 1 Ti coatings were deposited on similar as well as vastly different substrate materials with different nozzle speeds while keeping other CGS parameters constant in this fundamental research. This should allow for examining the interaction or inter-dependencies between coating and substrate materials in CGS, with the focus on determining the contribution of the thermal effect on the residual stresses. Thin substrates (3 mm thickness) in this case also allow to analyse the residual stress driven distortions in coating-substrate assemblies, which subsequently lead to the modified final residual stress state. Thus, the present work can be used in optimizing the cold gas spraying conditions for better material deposition quality, especially in case of depositing coatings or repairing thin structures and possibly transferring the knowledge to the real repair applications for aerospace components at a later stage. Under this aim, the CGS process parameter nozzle traverse speed was systematically varied to allow for changes to the thermal history and to the local temperature gradients.

In general, the residual stress analysis methods are mainly categorized by (i) diffraction methods (i.e., x-ray/synchrotron x-ray diffraction and neutron diffraction), (ii) mechanical/relaxation measurement methods (i.e. hole-drilling, slitting, and contour method), and (iii) other methods (i.e., magnetic, ultrasonic, thermoelastic, and photoelastic) (Ref 28). The choice of methods for residual stress determination depends on several factors as listed in (Ref 29). The diffraction methods are some of the most commonly used methods for residual stress analysis. However, soft x-rays produced in conventional x-ray tubes (photon energies < 20 keV) can only be used to determine residual stress at the surface due to penetration depths only reaching up some micrometres in case of metals (depending on the absorption coefficient of the material and the beam path geometry). Higher photon energies for x-rays that provide much higher information depth are typically sourced from large scale facilities, i.e., at synchrotron storage rings. However, the access to these high brilliance x-ray sources or also to neutron source, which also provide higher information depths and therefore enable for non-destructive analysing residual stresses in larger depth, is very limited. Moreover, diffraction methods are also sensitive to microstructure (i.e., grain size and to crystallographic texture). Conversely, above-mentioned mechanical methods are capable to analyse residual stress depth gradients. For example, the incremental hole-drilling method is fast, standardized, and mostly insensitive to grain size and crystallographic texture. By means of incremental hole-drilling, the depth distribution of the plane stress state can be reliably determined in the near-surface region up to the depth similar to about 65–70% of the hole diameter (Ref 30), which fits well to determine through-thickness residual stress depth distribution in CGS deposited coatings, and in the substrate through the interface. In the incremental hole-drilling method (ASTM E837 standard), a non-uniform residual stress depth profile is measured by introducing a small blind hole in certain number of drilling steps (increments) and the strain relaxations occur on the surface, as a result of removing stressed material, are recorded at each drilling step (Ref 31). The residual stress state in the sample is then determined from the measured strain relaxation by using particular evaluation methods. For instance, the integral method (Ref 32, 33) and the differential method (Ref 30) are among the commonly used methods for evaluating residual stresses from measured strain relaxation in incremental hole-drilling. The

incremental hole-drilling method can also determine residual stress distributions in coating–substrate composite (coating material different from substrate) by determining case-specific calibration coefficients using finite element simulations (Ref 34, 35). Residual stresses in the present study of CGS deposited coatings comprise of deposition stresses and thermal stresses caused by differential thermal contraction of coating and substrate during cooling down. Therefore, the residual stress depth profiles in this study are determined by means of incremental hole-drilling.

In addition to the finely resolved analysis of residual stress depth gradients within the coatings, complementary analysis of the surface topography of as-sprayed samples and of the microstructure was done to examine the coating quality such as morphological characteristics of as-sprayed coating surface and the porosity (or density) in the deposited material, respectively.

Materials and Methods

Materials

The present work focuses on grade 1 Ti (Ti99.7) coatings deposited on the substrates of different materials, namely grade 2 Ti, austenitic stainless steel (AISI304), and commercially pure (CP) copper using cold gas spraying. In order to avoid additional sources that could contribute to the build-up of residual stresses, the substrates were used in as-delivered conditions and only degreased with acetone before deposition. The material-specific data considered for residual stress evaluations in this study for Ti (grade 1 and 2), CP copper and steel-AISI304 are given in Table 1. The feedstock powder of grade 1 Ti from Eckart TLS GmbH, Germany, was used for producing CGS coatings. Figure 1(a) and (b) display the powder morphology and the cumulative particle size distribution of the powder, respectively. The feedstock powder particles were almost spherical in shape, and the particle sizes were mostly in the range of 32–45 µm. The dimensions of substrates are 70 mm × 50 mm × 3 mm in length × width × thickness. However, the area on which the coatings were produced is 50 × 50 mm^2 as shown in Fig. 2(c). As the overall focus is to enhance the performance of components used in lightweight applications (i.e., aerospace applications), thin sheet metal (thickness: 3 mm) substrates were prioritized in this study.

Cold Gas Spraying

A CGS system EvoCSII (Impact gun 6/11) from Impact innovation GmbH, Germany, was employed for depositing the material, enabling gas pressures and temperatures of up to 50 bar/1100 °C or 60 bar/1000 °C. In this study, nitrogen was used as process gas at 1100 °C temperature (T_{gas}) and 45 bar pressure (P_{gas}) for depositing grade 1 Ti coatings of approximately 1 mm in thickness. The parameters were chosen based on elaborate pre-studies. The setup holding the substrates for CGS deposition is illustrated in Fig. 2(a and b). Figure 2(b) shows that the substrates are clamped only from one end keeping the other end free in order for avoiding external stresses under thermal expansion. In Fig. 2(a), four substrates are clamped at the bottom end using a metal plate, while a similar plate at the top end was used only as free-standing mask for protecting a similar area from deposition, here keeping symmetric deposit-substrate conditions. The deposition of particles was performed in a direction normal (spray angle: 90°) to the substrate surface with 40 mm stand-off distance between nozzle outlet and substrate. The coatings were sprayed by the nozzle moving in a meandric scan pattern with 2 mm distance between two adjacent lines as shown in Fig. 2(d).

The nozzle traverse (scanning) speed is one of the key CGS parameters affecting the residual stress development. Therefore, in order to investigate the influence of nozzle traverse speed on residual stresses due to varying local temperature gradient for different nozzle speeds, three different speeds of nozzle: 125 mm/s, 250 mm/s, and 500 mm/s were considered. It is obvious that at a lower nozzle speed more material is deposited per pass. Therefore, to keep the thickness of the coatings similar, the number of passes were adapted for different nozzle speeds as shown in Table 2. The aimed thicknesses of the coatings were 1 mm. The coating–substrate cross-section images taken at the light optical microscope were used to measure the actual coating thicknesses mentioned in Table 2.

Analyses of Surface Topography and Microstructure

The surface topographies of as-sprayed coatings were measured by confocal microscope µSurf® from NanoFocus AG, Germany, with 10 x magnification. One measurement

Table 1. Material-specific data utilised for residual stress evaluation in the current study for Ti (grade 1 and 2), CP copper, and austenitic steel-AISI304

Material	Young's modulus [GPa]	Poisson's ratio	CTE at 20 °C [µm/m-°C]
Grade 1 Titanium	105	0.37	8.6
Grade 2 Titanium	105	0.37	8.6
CP copper	120	0.34	16.4
Steel-AISI304	200	0.29	17.3

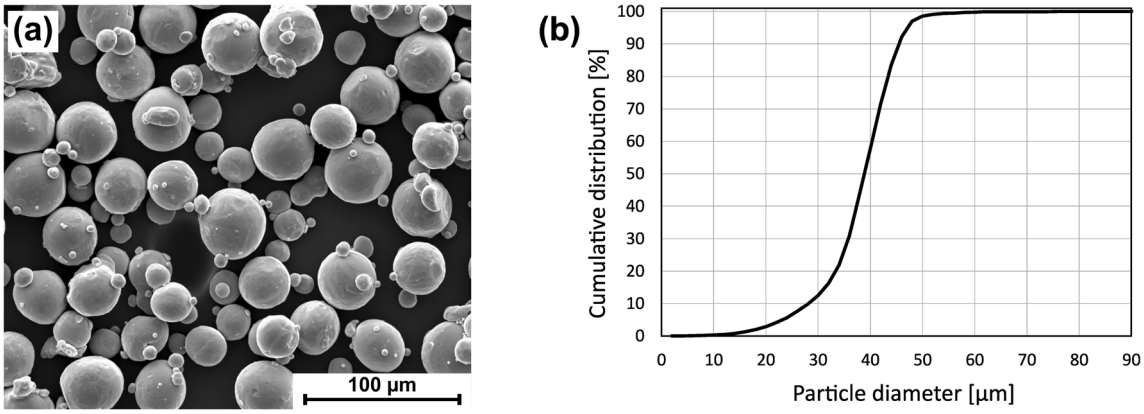

Fig. 1 (a) Morphology of the grade 1 Ti powder feedstock and (b) the respective cumulative particle size distribution

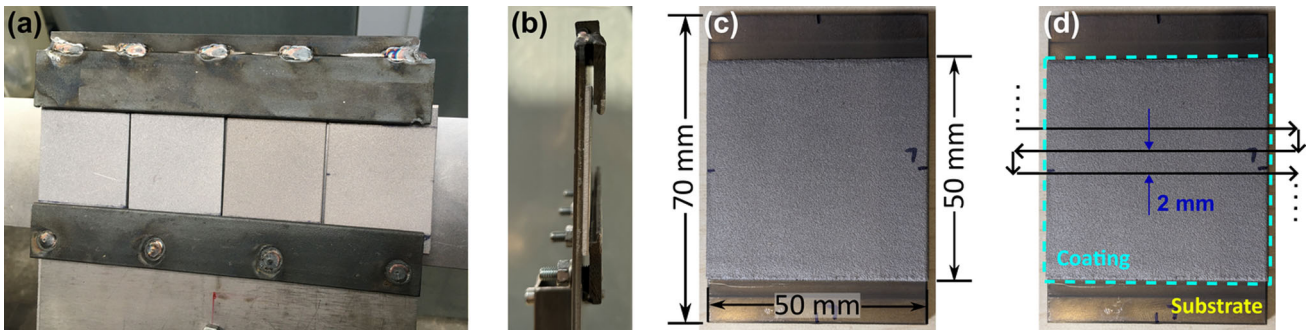

Fig. 2 Substrate arrangement and deposition condition. (a, b) the substrate holder holding four substrates, (b) substrates clamped from the bottom and free on top, (c) the dimensions of the substrate and the sprayed region, and (d) indicating part of the spray pattern with a 2 mm line distance between two adjacent lines of the meandric scanning style nozzle trajectory

Table 2. Parameters for depositing Grade 1 Ti coatings on grade 2 Ti, AISI304, and commercially pure (CP) Cu substrates with different nozzle traverse speeds.

Substrate material	Nozzle traverse speed [mm/s]	Number of passes	Total coating thickness [mm]	Coating thickness per pass [mm]
Grade 2 Titanium	125	2	1.092	0.546
	250	4	0.994	0.249
	500	8	0.952	0.119
Austenitic steel (AISI304)	125	2	–	–
	250	4	0.924	0.231
	500	8	1.032	0.129
Commercially pure (CP) copper	125	2	–	–
	250	4	0.983	0.246
	500	8	1.098	0.137

The stand-off distance, gas temperature, and pressure were 40 mm, 1100 °C, and 45 bar, respectively. The thicknesses of the coatings on AISI304 and CP copper substrates with 125 mm/s nozzle speed (2 passes) are not mentioned as the coatings in these cases were delaminated and therefore excluded from the current study

per sample over a 3 × 3 mm^2 area of the as-sprayed surface was performed. Only primary profiles of the surfaces were analysed and plotted. However, the underlying shape (or form) of the surface was removed from the measured

data. Since the samples appeared to be slightly bent in an as-sprayed condition, the 2nd-order polynomial surface fit was derived as a reference geometry (underlying shape) and removed from the measured data before plotting.

Furthermore, the light optical microscope images of the coating–substrate cross sections at 50x magnification were taken by a Zeiss Axiovert 200 MAT inverted microscope from Carl Zeiss Microscopy GmbH, Germany. The sample preparation for optical microscopy includes wet grinding of the embedded subsample started with P320 SiC paper and continued with P600, P1000, and P2500 SiC papers. After grinding, the rough polishing with 9 µm diamond paste and the final active oxide polishing with colloidal silica suspension (OP-S) containing H_2O_2 was carried out. The porosity was quantified from micrographs (2D analysis) using an image processing program Fiji (Ref 36). The porosity was determined as an area fraction in a (thresholded) binary image of a coating segment of the micrograph.

Residual Stress Analysis: Incremental Hole-Drilling

In the previous section, the incremental hole-drilling and the methods for evaluation of residual stress from the measured data were described. However, the standard calibration data developed for the evaluation of residual stress in homogeneous materials (homogeneous distribution of elastic properties in depths) is not suited for composite material systems, i.e., the mechanical properties of coating and substrate materials are different. Therefore, in case of grade 1 Ti coatings on steel (AISI304) and CP copper substrates in this study, the case-specific calibration data were determined explicitly by a three-dimensional finite element (FEM) model of incremental hole-drilling using Abaqus CAE software. In the FEM model, the different elastic properties were assigned to the coating and substrate and the perfect bonding between coating and substrate was assumed. Considering the axis-symmetry state, only a quarter of a model was used for simulation (Ref 34, 35).

Furthermore, instead of standard centre hole-drilling, an orbital drilling technique was employed. In orbital drilling, a smaller drill, positioned at an offset, orbits in a circular motion, producing a hole of a similar size to that drilled by a conventional centre hole-drilling using a larger drill (Ref 37). An in-house device, featuring a high-speed air turbine facilitated by an orbital motion, was employed for incremental hole-drilling. The drilling depth increments were controlled by a stepper motor. Six-blade TiN-coated tungsten carbide end mill bits of 0.8 mm nominal diameter were used for introducing a hole in an orbital manner, aiming for diameters of nominally 1.7 mm. At the end of drilling, the diameter of the hole was measured by optical means. The ASTM standard type B strain gauge rosettes (CEA-06-062UM-120) from Micro-Measurements (a Vishay Precision Group brand) with three strain gauge elements and a nominal gauge diameter of 5.13 mm, were utilized for the measurement of strain relaxations caused by the material removal. The notable roughness of a coating surface in an as-sprayed condition causes difficulties in gluing the strain gauge rosette properly and subsequently leads to incorrect strain measurements. Therefore, the deposited coating surfaces were locally ground carefully to enable improved attachment of the strain gauges. The careful grinding was done using P320, P600, and P1000 SiC grinding papers. Ethanol was dripped regularly onto the coating surface for cooling during the grinding. To mitigate the influence of grinding on residual stress state, the grinding was performed manually to avoid applying excessive pressure.

Typical measurement uncertainties for application of the incremental hole-drilling method are described in (Ref 37). Following (Ref 37), some of the uncertainty sources, for example, include uncertainty of measuring strain relaxations and reaching exact targeted drilling depth increment as well as operator skills and the properties of material itself. For steels, as an example in (Ref 37), with a residual stress depth gradient from about 260 MPa (near surface) to about 115 MPa (at increasing depths) over the depth range of 1 mm, the uncertainty in calculated residual stress reached about ± 40 MPa close to the surface (first 100-200 µm) and was much smaller (about ± 12 to ± 24 MPa) for increasing depths. Hence, for materials with lower stiffness (e.g., Ti-based-alloys) and similar residual stress levels results in higher strain relaxations during hole-drilling, leading to a smaller absolute uncertainty, as a result of reduced hole-drilling strain sensitivity, in comparison to steel as considered in (Ref 37). For the results presented in this work, we assume a maximum uncertainty for the residual stresses of about ± 20 MPa occurring for the highest residual stress levels measured and the mean uncertainty is estimated to reach about 10% of the present (lower) stress levels.

Simulation

The thermal history for different nozzle traverse speeds was obtained by finite element modelling, using a heat transfer model within the ABAQUS software. Substrate and coating dimensions were considered as in real part dimensions with thicknesses of 3 mm and 1 mm, respectively. The model assembly was assumed to interact with the environment through convection. The simulations were performed for titanium as a coating and the substrate materials. Therein, it was assumed that the titanium

coatings have the same thermal properties as the respective bulk material.

The heat transfer parameters given by the heat transfer coefficient (h) and the value of heat flux were obtained as described in (Ref 20), by tuning the parameters until the simulation results fit the experimentally observed temperatures. The thermal history was measured at the centre of the coating area, in the substrate close underneath (1 mm below) the coating–substrate interface. Experimentally, the thermal history was measured in situ by inserting a thermocouple in the substrate at the above-mentioned location through a small hole made at the back side of the substrate. The heat transfer parameters in the simulation were varied until reaching the best fit between the modelled and the measured thermal history for this specific cold spraying condition. Subsequently, the estimated heat input and heat transfer coefficient were used in the following FEM simulations to study the influence of different nozzle traverse speed by changing heating and cooling time in accordance with the experiments.

Results and Discussion

Surface Topography and Microstructure

Figure 3(b), (c), and (d) shows the 3D colour mappings (top view) illustrating the surface topography of as-sprayed grade 1 Ti coatings on grade 2 Ti substrates deposited with nozzle traverse speed 125 mm/s, 250 mm/s, and 500 mm/s, respectively. The 3×3 mm^2 coating area over which the surface topography was measured is indicated in Fig. 3(a) as a size reference. The measurement location may differ from that shown in Fig. 3(a). The plots shown in Fig. 3 are the contour plots of optical 3D surface measurements in which the colour bars on the right side of each plot indicate the z-coordinates (out of the page direction) or height in μm. The other coating systems included in this study, such as grade 1 Ti coating on CP copper and steel-AISI304 substrates, also exhibited similar surface topographies to the ones shown in Fig. 3. In general, the CGS deposited components require post-processing such as milling, grinding or polishing in order to produce a smooth functional surface. Therefore, the surface topography of as-sprayed samples indicates the amount of essential post-processing. However, the nozzle speed (i.e., 125, 250, and 500 mm/s) does not seem to have a significant influence on the topography of as-sprayed surfaces, as can be seen by the results presented in Fig. 3. Moreover, the post-processing of the as-sprayed components is not the focus of these fundamental investigations.

Figure 4(a), (b), and (c) shows the coating–substrate cross-section micrographs of grade 1 Ti coatings on grade 2 Ti substrates deposited with different nozzle traverse speeds: 125, 250, and 500 mm/s, respectively; and Fig. 4(d), (e), and (f), respectively, indicate the cross-section micrographs of grade 1 Ti coatings deposited on different substrate materials: CP copper, grade 2 Ti and steel-AISI304 with same nozzle traverse speed 250 mm/s. Figure 4(b) and (e) are identical and repeated to improve clarity, as the top row shows the comparison of coating microstructure for different nozzle speeds, and the bottom row illustrates the comparison of coating microstructure for different substrate materials. The coating microstructures exhibit lower porosity, which appears to account for approximately 2% area fraction of the micrographs (only coating segment) in case of grade 2 Ti substrate for all three nozzle speeds and about 1% area fraction in case of CP copper and steel-AISI304 substrates. The thickness of the coatings seems to differ slightly, especially with the nozzle traverse speeds and also in case of AISI304 substrate, i.e., Fig. 4(f). Varied coating thicknesses might result from the difference in deposition efficiency with respect to nozzle traverse speed and substrate material properties. However, deposition efficiency analysis and further analysis concerning the influence of nozzle speed and substrate material on the porosity and coating microstructure is beyond the scope of the present study.

Residual Stresses

The coatings produced with travers speeds of 125 mm/s onto CP copper and steel-AISI304 substrate were partially delaminated during the deposition process, as shown in Fig. 5(a) and (b), respectively, which may cause considerable residual stress relaxation and therefore, are not considered for the discussion of the residual stress states built up due to CGS. The delamination of the above-mentioned coatings for 125 mm/s nozzle speeds might be attributed to a higher CTE difference and higher localized heat input due to a slower movement of the heat source. The latter could cause more tensile deposition stresses, especially at the beginning when the substrate surfaces are roughly at room temperature.

Figure 6 displays the residual stresses over depth in two in-plane directions (transverse: along the nozzle scanning and longitudinal: 90° to the nozzle scanning) for grade 1 Ti coating deposited on grade 2 Ti substrate with a nozzle speed of 500 mm/s. The longitudinal and transverse directions with reference to a sample geometry are indicated in Fig. 6. The same also applies to the subsequent residual stress results presented later in this paper. The plot in Fig. 6 shows that the residual stresses determined up to a depth of approximately 1.1 mm are tensile in nature, ranging between about 30 and 80 MPa. Moreover, the residual stresses were mostly homogeneous, showing no significant change over depth (except for the values close

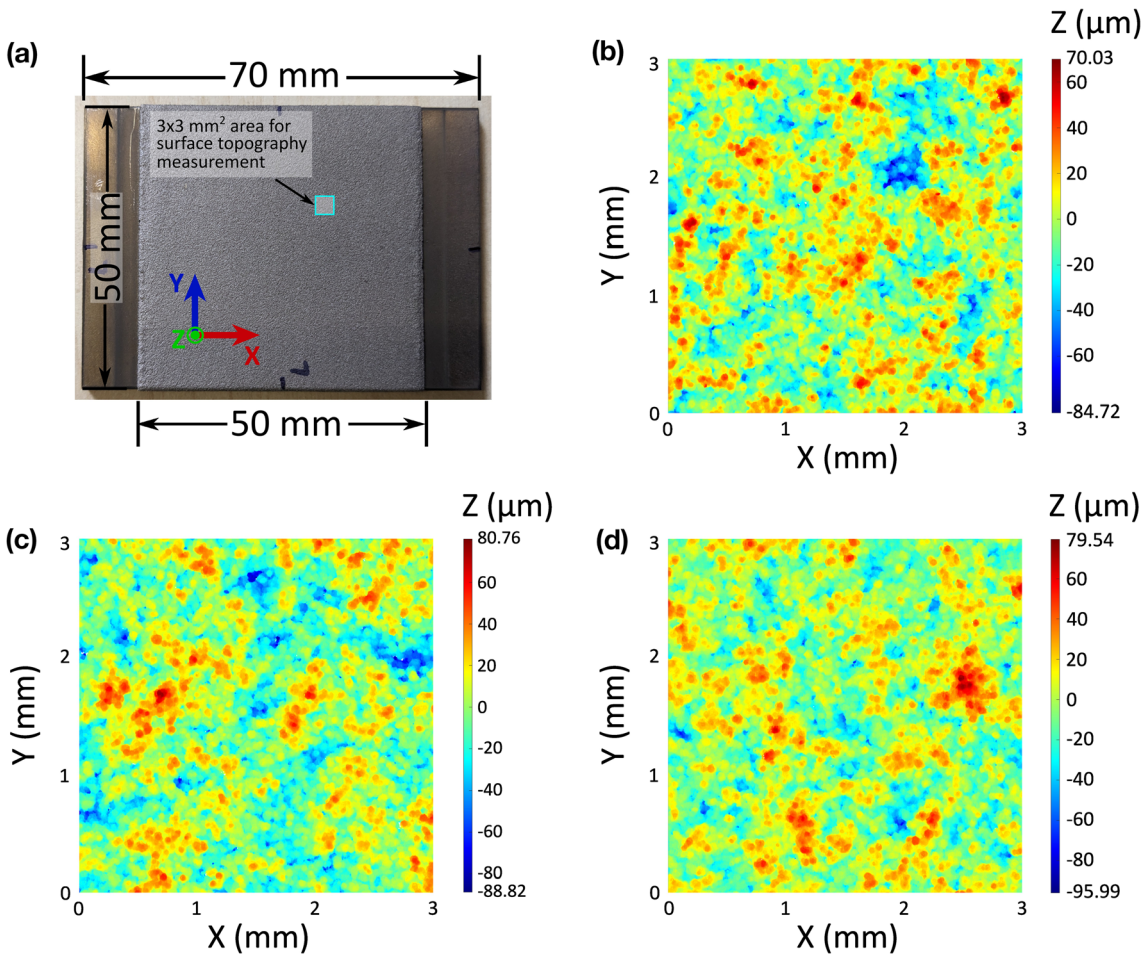

Fig. 3 (a) Sample geometry and a 3×3 mm^2 area on the coating surface as a reference example. The surface topographies of a 3×3 mm^2 area of as-sprayed grade 1 Ti coatings on grade 2 Ti substrates sprayed with CGS parameters T_{gas}: 1100 °C, P_{gas}: 45 bar and nozzle speed: (b) 125 mm/s, (c) 250 mm/s, and (d) 500 mm/s

to the surface). Furthermore, a slight directional dependency in the residual stress state over the depth can be shown in Fig. 6, indicating the residual stresses in transverse direction (along the nozzle scanning direction) being higher than in longitudinal direction.

On the one hand, this might result from the spraying setup constraints. For instance, the substrates, as shown in Fig. 2(b), were clamped at one end and the other end was free, restricting the substrate deformation in transverse direction. On the other hand, such could be induced by difference in local temperature gradients (spatial temperature distribution) in longitudinal and transverse direction caused as a result of the nozzle scanning pattern. In addition, the slightly different component stiffness in longitudinal and transverse direction resulting from the rectangular substrate dimensions (length: 70 mm and width: 50 mm) might also influence the direction dependence of the residual stress state. Since thermal expansion coefficients are the same for coating and substrate (Ti coating on Ti substrate), final stresses are seemingly dominated by local temperature gradient effects (and not the peening effects) during deposition. In some papers, this is referred to as a 'quenching effect' which is actually a complex context and may not be clearly expressed by the term 'quenching', in which the local temperature balance, taking into account the local heat conduction and the local thermal yield strength, plays a decisive role. In (Ref 10), the residual stresses in cold gas sprayed Ti-6Al-4V coatings on Ti-6Al-4V substrate deposited with similar process parameters (1100 °C gas temperature and 50 bar gas pressure) analysed by neutron diffraction and contour method, were also found to be tensile in the coatings.

Figure 7 illustrates the residual stress depth distributions in grade 1 Ti coatings sprayed on grade 2 Ti substrates with nozzle speeds of 125 mm/s, 250 mm/s, and 500 mm/s in 7(a) longitudinal and 7(b) transverse direction. In Fig. 7, the residual stresses in the coatings are observed to be more tensile when sprayed with lower nozzle speeds, i.e., the residual stresses become more tensile as the nozzle speed decreases. This implies that the thermal gradient effect is

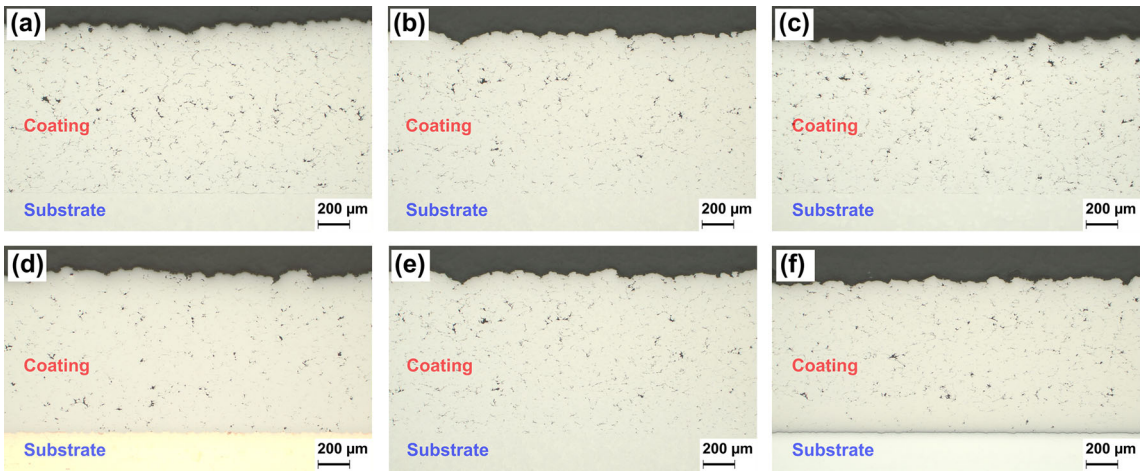

Fig. 4 Cross-sectional micrographs of cold gas sprayed grade 1 Ti coatings. Top row: coatings deposited on grade 2 Ti substrates with (a) 125 mm/s, (b) 250 mm/s, and (c) 500 mm/s nozzle speed. Bottom row: coatings deposited on (d) CP copper, (e) grade 2 Ti, and (f) steel-AISI304 substrate with the same 250 mm/s nozzle speed. Subfigures (b) and (e) are identical and intentionally repeated to enhance clarity, as the top row compares coating microstructure for different nozzle speeds and the bottom row compares the coating microstructure for different substrate materials. The process gas temperature and pressure for all coatings were 1100 °C and 45 bar, respectively

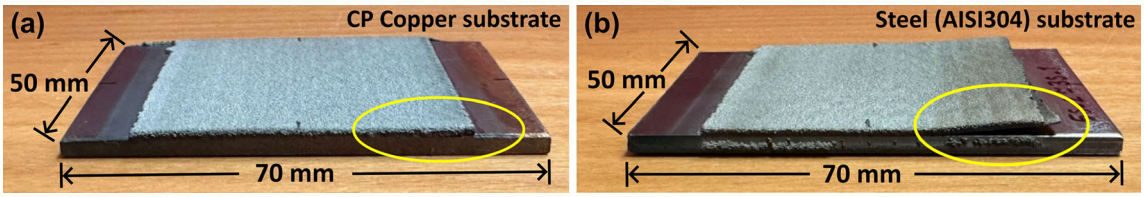

Fig. 5 Delaminated grade 1 Ti coatings deposited on (a) CP copper and (b) steel-AISI304 substrates with 125 mm/s nozzle speed, 1100 °C gas temperature, and 45 bar gas pressure

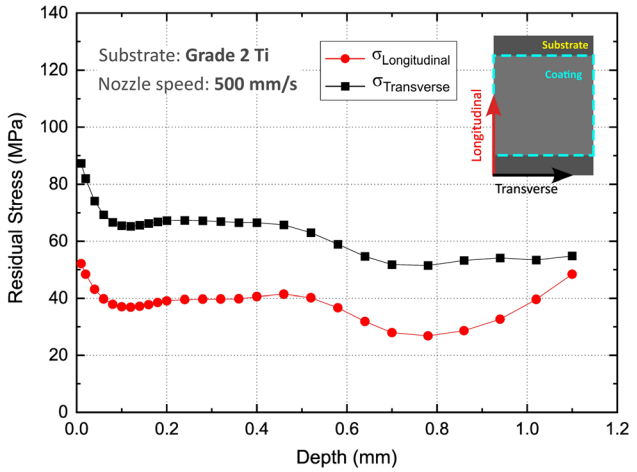

Fig. 6 Residual stress depth distribution in CGS deposited (T_{gas}: 1100 °C, P_{gas}: 45 bar and nozzle speed: 500 mm/s) grade 1 Ti coating on grade 2 Ti substrate in longitudinal and transverse direction

more pronounced as the local heat input is higher when the nozzle travels slower and vice versa. The higher nozzle speed allows for a more even heat distribution due to the changed heat input and additionally a more efficient heat dissipation, thereby reducing the significance of local temperature gradient effect (Ref 25). This issue is more understandable by looking at the thermal history of the parts for different nozzle speeds (Fig. 8). According to the thermal history graphs in Fig. 8, as the nozzle traverse speed decreases, the temperature in the substrate close underneath the coating (1 mm below the coating–substrate interface) increases due to longer duration of local heating on the component (increasing the thermal input). This indicates that a lower nozzle traverse speed increases local temperature and shifts the residual stress distributions toward a more tensile state. Furthermore, the number of peaks in the temperature history shown in Fig. 8 corresponds to the number of passes for each nozzle speed case. Ideally, the time required for spraying approximately 1 mm thick coatings with each nozzle speed (i.e., 125, 250, and 500 mm/s) should be similar, as the number of passes was adapted accordingly. However, it does not correspond with the temperature history shown in Fig. 8 for different nozzle

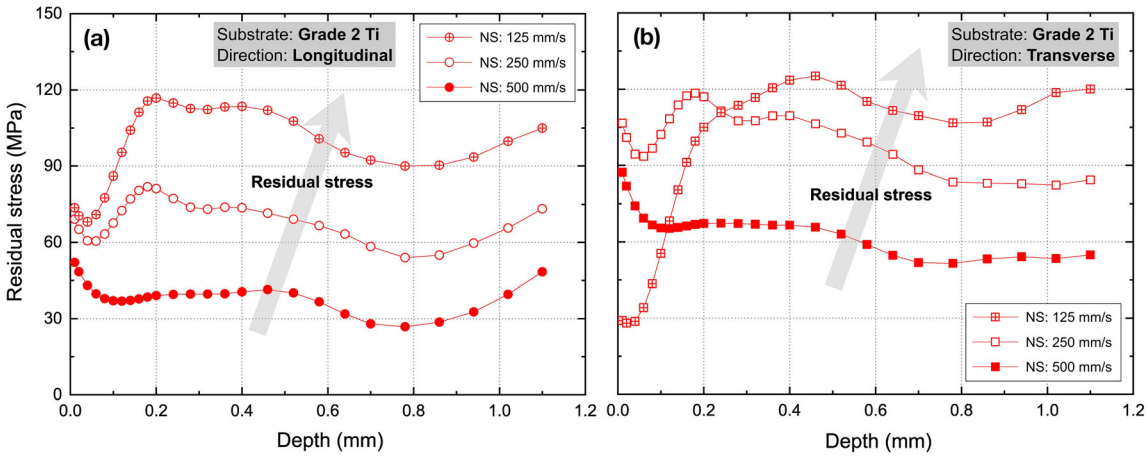

Fig. 7 Residual stress distribution in grade 1 Ti coatings deposited on grade 2 Ti substrates with different nozzle speeds (NS: 125, 250, and 500 mm/s) in (a) longitudinal and (b) transverse direction

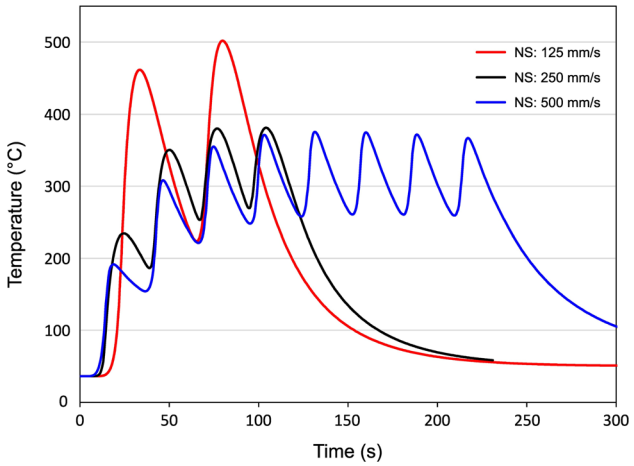

Fig. 8 Thermal history of grade 2 Ti substrate with different nozzle traverse speeds: 125, 250, and 500 mm/s

speeds, as 500 mm/s nozzle speed appears to have taken a longer time for spraying than 125 mm/s nozzle speed. This is due to the fact that the spraying nozzle, in each case, was made to traverse an extra distance to the left and right side of the substrate during travelling each line of the scanning pattern to accommodate acceleration and deceleration of the nozzle at the beginning and end of the line, respectively. Therefore, a greater number of passes (even with higher nozzle speed) results in longer overall time required for spraying the coating, as shown in Fig. 8.

In incremental hole-drilling, the smaller drilling increments near the surface (first increments) exhibit high uncertainties in released strain, and one of the reasons for that might be attributed to the end mill shape, which shows small chamfers (Ref 38) that are usually not considered when calculating the calibration functions or coefficients. Furthermore, the component's surface roughness might also lead to irregular strain relaxations due to less material removed during the first increments compared to the drilling in bulk material. This might affect the first two drilling increments. This point must be discussed together with setting the drilling depth z = 0. Due to surface roughness and slight local inclination of the normal to the surface relative to the drilling axis, the accurate determination of the surface (z = 0) is difficult as it is based on the light optical assessment of the surface after scratching the measuring point with the end mill while setting up the measurement. Furthermore, due to small drilling increments near the surface and small strain relaxations recorded by the strain gauges, the relative measurement uncertainties are expected to be higher than for larger drilling depths. These factors influence the subsequent residual stress evaluation near the surface and might contribute to the strong gradients in the near-surface residual stress depth distributions, in contrast to the coating interior, as can be seen in Fig 7. Apart from that, even though the surfaces of the CGS deposited coatings are only partially ground very carefully for incremental hole-drilling application (to allow for a proper strain gauge application), some roughness persists as shown in Fig. 9, potentially affecting the strain relaxations during near-surface drilling increments.

Figure 10 shows residual stresses determined in grade 1 Ti coatings deposited on steel (AISI304) and CP copper substrates for different nozzle speeds: 250 mm/s and 500 mm/s. Unlike grade 1 Ti coatings on grade 2 Ti substrates, these coating systems exhibit mostly compressive residual stresses of up to − 100 MPa in Ti coatings on copper substrates and − 160 MPa in Ti coatings on steel substrates, approximately. This might be associated with the significant difference between the CTEs of grade 1 Ti coatings and both steel-AISI304 and CP copper substrates. Therefore, compressive thermal stresses resulting from

different contractions of coating and substrate materials could exceed the deposition stresses (peening and local temperature gradient effects) and dominate the final residual stress state.

It is obvious that all residual stress distributions presented in Fig. 10 show a gradient which is similar to the thermal stress distribution typically observed in uniformly heated bimetallic sheets resulting from the internal force and moment balance due to misfit strain and adapted curvature of the sample (Ref 39). It means that the coated 3 mm thick CP Cu and AISI304 substrates show a slight but noticeable bending in convex shape, with the coating being at the outer side of the convex shape. Keeping one end of the sample loose (cf. Fig. 2), such should be due only to the internal stress distributions of the coating–substrate system. The residual stress distributions in Fig. 10 depict that the residual stresses increase to more compressive with the depth approaching the coating–substrate interface and near the interface to the substrate, the minimum in stress profiles indicates the highest compressive stress contributions. Similar to the case of grade 2 Ti substrates shown in Fig. 7, the lower nozzle speeds in Ti coatings deposited on CP copper and AISI304 substrates also shift the residual stress distributions more toward the tensile (or less compressive) regime (Fig. 10). Furthermore, despite having almost similar CTEs for AISI304 and CP copper substrates, Fig. 10 indicates different residual stress levels in grade 1 Ti coatings on these substrates deposited with identical process parameters. This could be assigned to different material properties of AISI304 and CP copper, such as thermal conductivity, heat capacity, strength, and stiffness. For instance, substrates undergo temperature cycles as the coating is progressively deposited and therefore, different thermal conductivity and specific heat capacity of CP copper and AISI304 substrates affect the temperature (and its gradient) of the substrates during deposition. Furthermore, different elastic strengths/stiffnesses of CP copper and AISI304 substrates lead to different stress states in the coating systems arising from internal force/moment balance (misfit strain). For example, higher stiffness of the AISI304 substrates in comparison to that of CP copper leads to higher compressive residual stresses in grade 1 Ti coatings as shown in Fig. 10. To provide more clear visual representation of the influence of nozzle speed on residual stresses, the residual stress values in transverse direction at only three depth steps in the coatings for different nozzle speeds are plotted in Fig. 11(a), (b), and (c) for grade 1 Ti coatings on grade 2 Ti, CP copper and steel-AISI304 substrates, respectively. It is important to note that the residual stress values plotted in Fig. 11 corresponding to different nozzle speeds and substrate materials are the same as shown in Fig. 7(b) and 10(b), but only at three distinct depths, namely, 320, 520, and 700 μm from the coating surface. As already explained, the role of nozzle speed in local heat input and temperature gradient, and therefore in residual stress development, Fig. 11 also clearly demonstrates that the increase in nozzle speed reduces the tensile or increases the compressive residual stresses built up in coatings.

Summary and Conclusions

This article presents the residual stress depth distributions in CGS sprayed grade 1 Ti coatings on 3 mm thick grade 2 Ti, CP copper, and austenitic stainless steel-AISI304 substrates determined by the incremental hole-drilling technique. The key findings of the investigation aimed at analysing the influence of nozzle speed and substrate material on the residual stress build-up in the CGS sprayed grade 1 Ti coatings are summarized as follows:

- In grade 1 Ti coatings deposited on grade 2 Ti substrates, the final residual stresses were tensile, and no thermal misfit stresses were expected due to the same CTEs. Here, the influence of local temperature gradient attributed to local heat input during deposition in CGS seems to hold a dominating role in residual stress development.
- The tensile residual stresses show an inverse correlation to nozzle speed (i.e., tensile stress in coating increases with decreasing nozzle speed). This implies that the

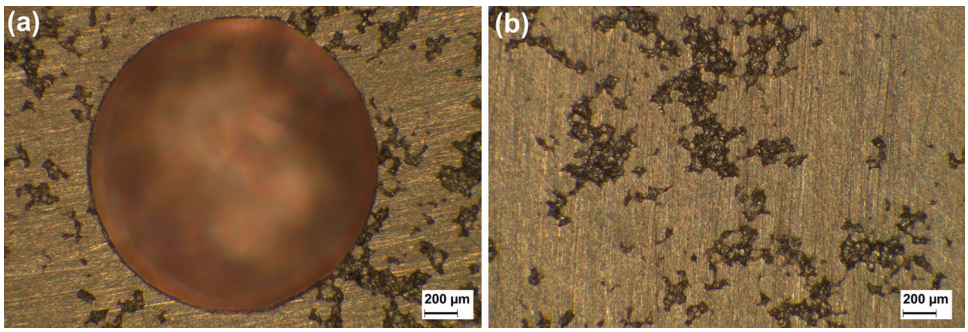

Fig. 9 (a) Top view of a hole drilled for residual stress analysis, and (b) other surface area close to the hole location in a grade 1 Ti coating deposited on CP Cu substrate with 500 mm/s nozzle speed, which shows the roughness remained after careful grinding

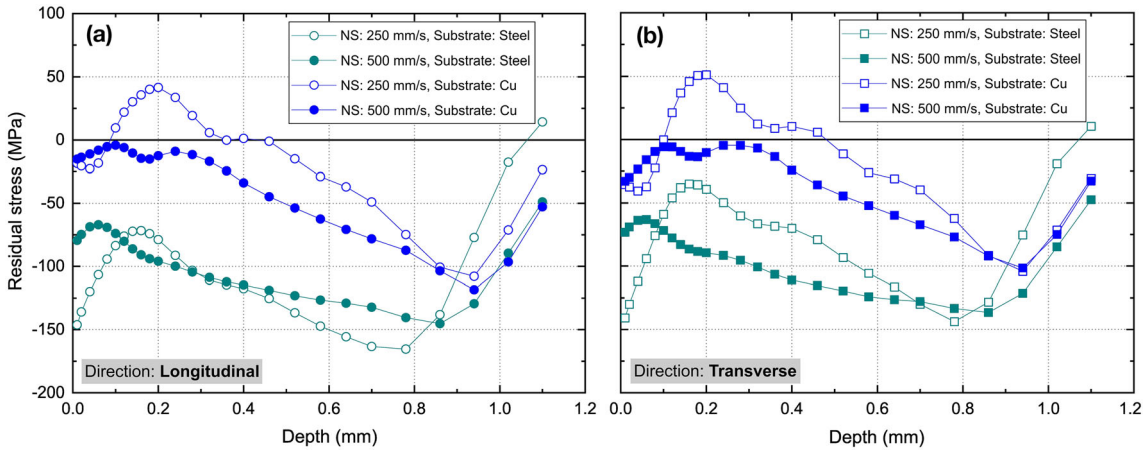

Fig. 10 Residual stress distribution in grade 1 Ti coatings deposited on steel-AISI304 (Steel) and CP copper (Cu) substrates with nozzle speeds 250 mm/s and 500 mm/s in (a) longitudinal and (b) transverse direction

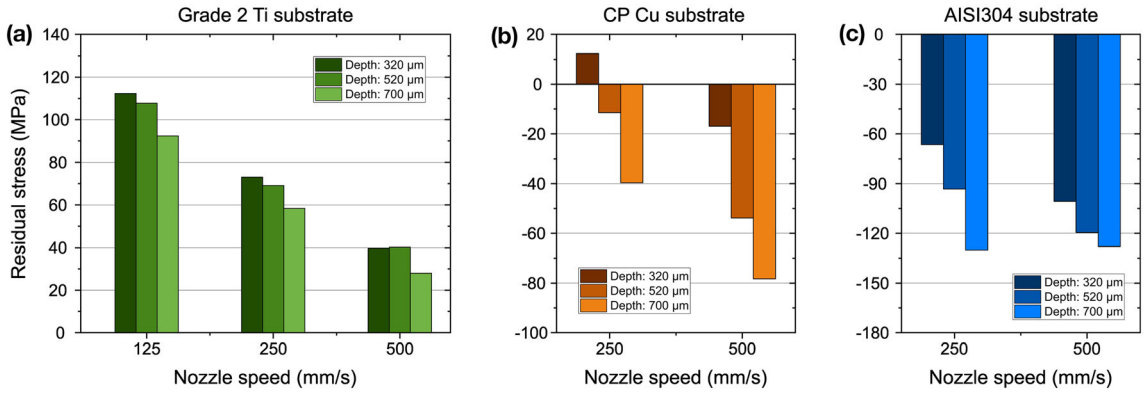

Fig. 11 Residual stress vs. nozzle speed at three depth steps 320, 520, and 700 µm from the coating surface in the transverse direction for the grade 1 Ti coatings deposited on (a) grade 2 Ti, (b) CP copper, and (c) AISI304 substrate

thermal effects get more pronounced as the nozzle travels at a lower speed.

- The residual stresses in the cold gas sprayed Ti coatings deposited on CP copper and AISI304 steel substrates are mostly compressive, in contrast to the results in case of grade 2 Ti substrate, which indicates that the thermal stresses generated due to differential contraction of coating and substrate materials during cooling are more pronounced compared to deposition stresses.
- Slight bending of CP copper and steel-AISI304 substrates (3 mm thick), potentially caused by the internal moment balance due to misfit strains upon cooling down, might contribute to a gradient in the residual stress depth distributions in coatings.
- Furthermore, the substrate material properties (i.e., heat conductivity, specific heat capacity, and stiffness) also influence the level of residual stresses developed in the coating. For instance, the higher stiffness of steel-AISI304 substrate than CP copper substrate results in the residual stresses in grade 1 Ti coatings being more compressive, even though the CTE values for both substrates are similar.

Acknowledgements This research in the frame of the project ''CORE—Computer-based Refurbishment'' is funded by dtec.bw—Digitalization and Technology Research Center of the Bundeswehr which we gratefully acknowledge. dtec.bw is funded by the European Union—NextGenerationEU.

Funding Open Access funding enabled and organized by Projekt DEAL.

References

1. P. King, M. Yandouzi, and B. Jodoin, The Physics of Cold Spray, *Modern Cold Spray: Materials, Process, and Applications*, 1st ed., J. Villafuerte, Ed., Springer Cham, 2015, p 31-72
2. M.F. Smith, Introduction to Cold Spray, *High Pressure Cold Spray: Principles and Applications*, C.M. Kay and J. Karthikeyan, Ed., ASM International, 2016, p 1-16
3. H. Assadi, F. Gärtner, T. Stoltenhoff and H. Kreye, Bonding Mechanism in Cold Gas Spraying, *Acta Mater.*, 2003, **51**(15), p 4379–4394.
4. T. Schmidt, F. Gärtner, H. Assadi and H. Kreye, Development of a Generalized Parameter Window for Cold Spray Deposition, *Acta Mater.*, 2006, **54**(3), p 729–742.
5. H. Assadi, H. Kreye, F. Gärtner and T. Klassen, Cold Spraying—a Materials Perspective, *Acta Mater.*, 2016, **116**, p 382–407.
6. A. Viscusi, A. Astarita, R. Della Gatta and F. Rubino, A Perspective Review on the Bonding Mechanisms in Cold Gas Dynamic Spray, *Surf. Eng.*, 2019, **35**(9), p 743–771.
7. T. Hussain, Cold Spraying of Titanium: A Review of Bonding Mechanisms, Microstructure and Properties, *Key Eng. Mater.*, 2013, **533**, p 53–90.
8. M. Grujicic, C.L. Zhao, W.S. DeRosset and D. Helfritch, Adiabatic Shear Instability based Mechanism for Particles/Substrate Bonding in the Cold-Gas Dynamic-Spray Process, *Mater. Des.*, 2004, **25**(8), p 681–688.
9. F. Gärtner, A. List, S. Nielsen, H. Wu, Z. Arabgol, L. Wiehler, J. Gutierrez de Frutos, C. Huang, T. Klassen, M. Lewke, A. Fay, D. Gabani, J. Gibmeier, A. Pundt, T. Werner, K. Hilgenberg, M. Madia, T. Böllinghaus, L. Holzgaßner, P. Richter, N. Clausing, H. Loitz, P. Keuter, M.t. Baben, M. Steierl, D.E. Schimbäck, T. Roßler, H. Debuch, T. Gartner, Computerized Refurbishment, *dtec.bw-Beiträge der Helmut-Schmidt-Universität / Universität der Bundeswehr Hamburg: Forschungsaktivitäten im Zentrum für Digitalisierungs- und Technologieforschung der Bundeswehr dtec.bw*, D. Schulz, A. Fay, W. Matiaske, and M. Schulz, Ed., 2022, p 9–19
10. D. Boruah, B. Ahmad, T.L. Lee, S. Kabra, A.K. Syed, P. McNutt, M. Doré and X. Zhang, Evaluation of Residual Stresses Induced by Cold Spraying of Ti-6Al-4V on Ti-6Al-4V Substrates, *Surf. Coat. Technol.*, 2019, **374**, p 591–602.
11. M. Lewke, S. Nielsen, A. List, F. Gartner, T. Klassen, and A. Fay, Knowledge-based Optimization of Cold Spray for Aircraft Component Repair, *2021 26th IEEE International Conference on Emerging Technologies and Factory Automation (ETFA)*, Sept 07-10, 2021 (Vasteras, Sweden), The Institute of Electrical and Electronics Engineers (IEEE) and IEEE Industrial Electronics Society (IES), 2021, p 1-4
12. W. Li, C. Cao and S. Yin, Solid-State Cold Spraying of Ti and its Alloys: A Literature Review, *Prog. Mater. Sci.*, 2020 https://doi.org/10.1016/j.pmatsci.2019.100633
13. R. Singh, S. Schruefer, S. Wilson, J. Gibmeier and R. Vassen, Influence of Coating Thickness on Residual Stress and Adhesion-Strength of Cold-Sprayed Inconel 718 Coatings, *Surf. Coat. Technol.*, 2018, **350**, p 64–73.
14. R. Vaßen, J. Fiebig, T. Kalfhaus, J. Gibmeier, A. Kostka and S. Schruefer, Correlation of Microstructure and Properties of Cold Gas Sprayed INCONEL 718 Coatings, *J. Therm. Spray Technol.*, 2020, **29**(6), p 1455–1465.
15. V. Luzin, A. Valarezo and S. Sampath, Through-Thickness Residual Stress Measurement in Metal and Ceramic Spray Coatings by Neutron Diffraction, *Mater. Sci. Forum*, 2008, **571–572**, p 315–320.
16. K. Spencer, V. Luzin, N. Matthews and M.X. Zhang, Residual Stresses in Cold Spray Al Coatings: the Effect of Alloying and of Process Parameters, *Surf. Coat. Technol.*, 2012, **206**(19–20), p 4249–4255.
17. F. Lang, J. Schmitt, S. Cabeza, T. Pirling, J. Fiebig, R. Vaßen, and J. Gibmeier, IN718 Cold Gas Repair Spray of Large Cavities—Microstructure and Residual Stresses, *Proceedings of the 10th International Symposium on Superalloy 718 and Derivatives*, 1st ed., E.A. Ott, J. Andersson, C. Sudbrack, Z. Bi, K. Bockenstedt, I. Dempster, M. Fahrmann, P. Jablonski, M. Kirka, X. Liu, D. Nagahama, T. Smith, M. Stockinger, and A. Wessman, Ed., May 14-17, 2023 (Pittsburgh, USA), Structural Materials Division and High Temperature Alloys Committee of The Minerals, Metals and Materials Society, Springer Cham, 2023, pp. 739-753
18. V. Luzin, K. Spencer, M. Zhang, N. Matthews, J. Davis, and M. Saleh, Residual stresses in cold spray coatings, *Cold-Spray Coatings: Recent Trends and Future perspectives*, 1st ed., P. Cavaliere, Ed., Springer Cham, 2018, pp. 451-480
19. V. Luzin, K. Spencer and M.X. Zhang, Residual Stress and Thermo-Mechanical Properties of COLD Spray metal Coatings, *Acta Mater.*, 2011, **59**(3), p 1259–1270.
20. Z. Arabgol, H. Assadi, T. Schmidt, F. Gärtner and T. Klassen, Analysis of Thermal History and Residual Stress in Cold-Sprayed Coatings, *J. Therm. Spray Technol.*, 2014, **23**(1–2), p 84–90.
21. J. Schmitt, J. Fiebig, S. Schrüfer, O. Guillon and R. Vaßen, Adjusting Residual Stresses During Cold Spray Deposition of IN718, *J. Therm. Spray Technol.*, 2024, **33**(1), p 210–220.
22. T. Suhonen, T. Varis, S. Dosta, M. Torrell and J.M. Guilemany, Residual Stress Development in Cold Sprayed Al, Cu and Ti Coatings, *Acta Mater.*, 2013, **61**(17), p 6329–6337.
23. S. Kuroda, Y. Tashiro, H. Yumoto, S. Taira, H. Fukanuma and S. Tobe, Peening Action and Residual Stresses in High-Velocity Oxygen Fuel Thermal Spraying of 316L Stainless Steel, *J. Therm. Spray Technol.*, 2001, **10**(2), p 367–374.
24. T.S. Price, P.H. Shipway and D.G. McCartney, Effect of Cold Spray Deposition of a Titanium Coating on Fatigue Behavior of a Titanium Alloy, *J. Therm. Spray Technol.*, 2006, **15**(4), p 507–512.
25. V. Luzin and D. Fraser, Neutron Through-Thickness Stress Measurements in two-Phase Coatings with High Spatial Resolution, *Mater. Res. Proc.*, 2018, **4**, p 111–116.
26. B. Marzbanrad, E. Toyserkani and H. Jahed, Customization of Residual Stress Induced in Cold Spray Printing, *J. Mater. Process. Technol.*, 2021 https://doi.org/10.1016/j.jmatprotec.2020.116928
27. V. Luzin, O. Kirstein, S.H. Zahiri and D. Fraser, Residual Stress Buildup in Ti Components Produced by Cold Spray Additive Manufacturing (CSAM), *J. Therm. Spray Technol.*, 2020, **29**(6), p 1498–1507.
28. P.J. Withers and H.K.D.H. Bhadeshia, Residual Stress Part 1-Measurement Techniques, *Mater. Sci. Technol.*, 2001, **17**(4), p 355–365.
29. G.S. Schajer and C.O. Ruud, Overview of Residual Stresses and Their Measurement, *Practical Residual Stress Measurement Methods*, G.S. Schajer, Ed., (John Wiley & Sons Ltd, 2013), pp. 1-27
30. T. Schwarz and H. Kockelmann, Die Bohrlochmethode - ein für viele Anwendungsbereiche optimales Verfahren zur experimentellen Ermittlung von Eigenspannungen, *Messtechnische Briefe*, 1993, **29**(2), p 33–38. ((**in German**))

31. Standard Test Method for Determining Residual Stresses by the Hole-Drilling Strain-Gage Method, ASTM E837 – 20, ASTM International, 2020
32. G.S. Schajer, Measurement of Non-uniform Residual Stresses using the Hole-Drilling Method. Part I-Stress Calculation Procedures, *J. Eng. Mater. Technol.*, 1988, **110**(4), p 338–343.
33. G.S. Schajer, Measurement of Non-uniform Residual Stresses using the Hole-Drilling Method. Part II-Practical Application of the Integral Method, *J. Eng. Mater. Technol.*, 1988, **110**(4), p 344–349.
34. E. Obelode and J. Gibmeier, Residual Stress Analysis on Thick Film Systems by the Incremental Hole-Drilling Method—Simulation and Experimental Results, *Exp. Mech.*, 2013, **53**(6), p 965–976.
35. E. Held and J. Gibmeier, Residual Stress Analysis of Thick Film Systems by the Incremental Hole-Drilling Method, *HTM J. Heat Treat. Mater.*, 2014, **69**(2), p 71–79.
36. J. Schindelin, I. Arganda-Carreras, E. Frise, V. Kaynig, M. Longair, T. Pietzsch, S. Preibisch, C. Rueden, S. Saalfeld, B. Schmid, J.Y. Tinevez, D.J. White, V. Hartenstein, K. Eliceiri, P. Tomancak and A. Cardona, Fiji: An Open-Source Platform for Biological-Image Analysis, *Nat. Methods*, 2012, **9**(7), p 676–682.
37. G.S. Schajer and P.S. Whitehead, Hole Drilling and Ring Coring, *Practical Residual Stress Measurement Methods*, G.S. Schajer, Ed., (John Wiley & Sons Ltd, 2013), pp. 29-64
38. A. Nau and B. Scholtes, Evaluation of the High-Speed Drilling Technique for the Incremental Hole-Drilling Method, *Exp. Mech.*, 2013, **53**(4), p 531–542.
39. S. Timoshenko, Analysis of bi-Metal Thermostats, *J. Opt. Soc. Am.*, 1925, **11**(3), p 233–255.